Circular RNA circBLNK promotes osteosarcoma progression and inhibits ferroptosis in osteosarcoma cells by sponging miR-188-3p and regulating GPX4 expression

ZHONGJUN LI[1*], YI LUO[2*], CHUNBO WANG[1*], DUNXIN HAN[1] and WEIPING SUN[1]

[1]Department of Orthopaedics, Weihai Medical District of The 970th Hospital of The PLA Joint Logistic Support Force, Weihai, Shandong 264200; [2]Department of Orthopaedics, The 970th Hospital of The PLA Joint Logistic Support Force, Yantai, Shandong 264002, P.R. China

Received November 10, 2022; Accepted July 4, 2023

DOI: 10.3892/or.2023.8629

Abstract. As a newly identified circular RNA (circRNA), the role of circBLNK in cancer progression has not been probed. The objective of the present study was to functionally dissect the role of circBLNK in osteosarcoma (OS) tumorigenesis and progression. With regards of the experimental procedure, the levels of mRNAs and proteins were assessed using reverse transcription-quantitative PCR and western blot analysis, respectively. The subcellular location of circBLNK in OS cells was determined by cell cytosolic/nuclear fractionation assay. Cell ferroptosis ability was assessed through MTT assay. Cell proliferative abilities were assessed by clonogenic and Cell Counting Kit-8 assays, and cell apoptosis was measured using flow cytometry. The relationships among circBLNK, miR-188-3p, and glutathione peroxidase 4 (GPX4) were validated by luciferase reporter and RNA pull-down assays, as well as RNA immunoprecipitation. The stability of circBLNK and linear BLNK was confirmed using RNase R treatment assay. The association between circBLNK expression and overall survival rate was assessed by Kaplan-Meier plot. The correlation between the expression levels of circBLNK, miR-188-3p, and GPX4 in OS tissues was assessed by Pearson's χ^2 test. The results revealed that CircBLNK and GPX4 were significantly upregulated in OS tissues, which predicted the poor prognosis. CircBLNK knockdown led to suppressed cell proliferation and enhanced cell apoptosis, an effect that could be reversed by the inhibition of miR-188-3p. In an *in vivo* circBLNK deficiency model, tumor growth was observed to be markedly suppressed. Moreover, circBLNK deficiency elevated levels of intracellular free iron (Fe^{2+}), malondialdehyde, lipid reactive oxygen species and mitochondrial superoxide, while diminishing mitochondrial membrane potential in Erastin-treated OS cells, which were eliminated by overexpressing GPX4. Furthermore, mechanistic investigations revealed that circBLNK sponged miR-188-3p to regulate the expression of GPX4, thereby affecting OS progression. In conclusion, the present study delineated a new regulatory axis involving circBLNK/miR-188-3p/GPX4 in OS progression, adding to the growing evidence that circRNAs are critical gene regulators in cancer progression.

Introduction

As a form of primary malignant bone tumor, osteosarcoma (OS) is ranked first in the cause of cancer-associated death in children and adolescents (1,2). OS is derived from mesenchymal cells, characterized by a high recurrence rate, early lung metastasis, and rapid infiltrating growth (3). Surgical resection, adjuvant chemotherapy, and small molecule targeted therapy have been used for OS treatment (4,5); however, because of the high propensity of metastasis and relapse the prognosis remains poor (6). Thus, it would be beneficial to identify novel OS therapies by studying complex gene regulatory networks. Circular RNAs (circRNAs) do not code for proteins and are characterized by a covalently closed loop (7). CircRNAs are resistant to RNA exonuclease digestion and therefore they are structurally stable (8). Through sponging miRNAs, circRNAs participate in the regulation of diverse cellular processes, such as cell division, apoptosis, migration and ferroptosis (9-12). CircRNAs exert vital functions in the progression of various cancers including OS. For instance, circRNA_103801 facilitates OS proliferation through regulating the miR-338-3p/HIF-1/Rap1/PI3K-Akt signaling pathway (13), circRNA_0008035 silencing represses OS metastasis by sponging miR-375 (14), and circMTO1 suppresses OS metastasis by regulating the miR-630/KLF6 signaling (15). CircBLNK is a newly discovered circRNA, located in chromosome 10, however, its functions in tumorigenesis remain understudied.

Correspondence to: Dr Dunxin Han or Dr Weiping Sun, Department of Orthopaedics, Weihai Medical District of The 970th Hospital of The PLA Joint Logistic Support Force, 8 Baoquan Road, Weihai, Shandong 264200, P.R. China
E-mail: 13573518855@163.com
E-mail: swp411@163.com

*Contributed equally

Key words: osteosarcoma, CircBLNK, microRNA-188-3p, glutathione peroxidase 4

MicroRNAs (miRNAs) are an abundant class of small non-coding RNAs with 18-24 nucleotides in length, typically acting as competing endogenous RNAs (ceRNAs) to suppress protein translation or promote mRNA decay (16). Numerous studies have implicated miRNAs in the regulation of tumorigenesis of malignancies. For instance, miR-151a-3p regulates OS cell proliferation by targeting RAB22A (17), miR-149 affects the tumorigenesis of OS through targeting MSI2 (18) and miR-16b promotes OS cell proliferation through regulating the PI3K/AKT signaling pathway (19). MiR-188-3p acts as a ceRNA in the tumorigenesis of various malignancies (20-22). However, whether miR-188-3p could regulate the tumorigenesis of OS remains unknown. Glutathione peroxidase 4 (GPX4) uses glutathione as a cofactor to deplete membrane phospholipid hydroperoxides, thereby maintaining cellular redox homeostasis (23). Abnormal activation of GPX4 can induce ferroptosis (24), a non-apoptotic form of cell death caused by iron-dependent accumulation of toxic lipid peroxides (25). Furthermore, GPX4 has been implicated in OS tumorigenesis (26,27). However, whether GPX4 could be targeted by miRNA to regulate OS tumorigenesis remains unstudied.

In the present study, the aim was to functionally dissect the role of circBLNK in OS progression and to delineate the relevant molecular mechanisms to gain new insights into the etiology of OS.

Materials and methods

Clinical tissue samples. Tissues of OS and non-cancerous regions were collected from 40 patients (age range, 16-54 years; mean age, 35±1.2 years; male/female ratio, 3:5) by surgery at the 970th hospital of the PLA Joint Logistic Support Force between August 2017 and June 2021. No chemotherapy or radiotherapy was applied to treat the patients before surgery. The tissue samples were verified by two pathologists. All patients were informed of the research design and written informed consent was provided by all patients. The present study was approved (approval no. EC-H-2021-12-16) by the Research Ethics Committee of the 970th hospital of the PLA Joint Logistic Support Force (Yantai, China), which was in accordance with the ethical standards formulated in the Helsinki Declaration (28).

Cell culture and transfection. The 293T cell line was purchased from the American Type Culture Collection, and four OS cell lines (HOS, SJSA-1, MG63 and U2OS) and the normal human osteoblast cell line (hFOB1.19) were obtained from ScienCell Research Laboratories, Inc. Cells were cultured in RPMI-1640 medium (HyClone; Cytiva) under a condition of 5% CO_2 and 37˚C. All media were supplemented with 10% (v/v) fetal bovine serum (FBS; MilliporeSigma), 100 IU/ml penicillin and 100 mg/ml streptomycin. Overexpression (OE)-vector, small interfering (si)-NC, si-circBLNK, OE-GPX4, inhibitor control, miR-188-3p inhibitor, mimic control, and miR-188-3p mimics were provided by Shanghai GeneChem Co., Ltd. Transfection of cells with a total of 20 nM of each indicated construct was implemented at 37˚C for 15 min using Lipofectamine® 3000 reagent (Invitrogen; Thermo Fisher Scientific, Inc.). After 48 h, the transfected cells were harvested to perform subsequent experiments. The sequences used were as follows: si-NC: 5'-TTCTCCGAACGTGTCACGT-3'; si-circBLNK#1: 5'-AGA TCTGTCTGAGAAGAAACA-3'; si-circBLNK#2: 5'-GAT CTGTCTGAGAAGAAACAA-3'; miR-NC mimic: 5'-GUC GUAUCCAGUGCAGGGUCC-3'; miR-188-3p mimic: 5'-CUC CCACAUGCAGGGUUUGCA-3'; miR-NC inhibitor: 5'-UUC UCCGAACGUGUCACGUTT-3'; miR-188-3p inhibitor: 5'-GAGGGUGUACGUCCCCAAACGU-3'.

RNase R treatment assay. Cytoplasmic and nuclear RNAs were separated using a cytoplasmic and nuclear RNA separation kit according to the manufacturer's protocol. Total RNAs were isolated by TRIzol® reagent (Invitrogen; Thermo Fisher Scientific, Inc.) from OS tissues and MG63 and U2OS cell lines according to the manufacturer's protocol. For RNase R assay, RNase R (3 U/mg; cat. no. ab286929; Abcam) was applied to the RNAs and incubated for 15 min at 37˚C. Afterwards, the remaining RNAs were assessed by reverse transcription-quantitative PCR (RT-qPCR).

RT-qPCR. Following RNA isolation by TRIzol® reagent from MG63 and U2OS cells, cDNA was synthesized by a High-Capacity cDNA Reverse Transcription kit (cat. no. 4368814; Thermo Fisher Scientific, Inc.) according to the manufacturer's instruction. The Thermal Cycler Dice System (Takara Bio, Inc.) with the SYBR Green PCR Master Mix (Thermo Fisher Scientific, Inc.) were used to perform qPCR. The reaction mixture was incubated at 95˚C for 2 min. The thermocycling program consisted of mainaining at 94˚C for 2 min, followed by 30 cycles of 30 sec at 94˚C, 30 sec at 56˚C, and 60 sec at 72˚C. The $2^{-\Delta\Delta Cq}$ method was employed to assess relative expression levels (29). The primers are listed in Table I.

Western blot analysis. The protein was extracted from MG63 and U2OS cells as previously described (30). Lysate samples (40 μg) were applied to a 10% SDS-PAGE gel, and following electrophoresis, the separated protein was transferred to a PVDF membrane (Invitrogen; Thermo Fisher Scientific, Inc.). After treatment with 5% skim milk at 37˚C for 2 h, the membrane was treated with anti-GPX4 (1:1,000; cat. no. ab125066; Abcam) and GAPDH (1:1,000; cat. no. 92310; Cell Signaling Technology, Inc.) at 4˚C for 24 h. Subsequently, the membrane was treated with the IgG H&L (HRP-conjugated; 1:10,000; cat. no. 7076S; Cell Signaling Technology, Inc.) at 37˚C for 2 h. The blot was finally developed by ECL reagents (Amersham; Cytiva), and the band intensity was measured using ImageJ version 4.1 (National Institutes of Health).

Cell cytosolic/nuclear fractionation assay. The nuclear and cytosolic fractions of MG63 and U2OS cells were separated using the Cytoplasmic & Nuclear RNA Purification Kit (100) (cat. no. NGB-37400; Norgen Biotek Corp.) according to the manufacturer's protocol. The RNA was extracted from the nuclear and cytosolic fractions. Afterwards, the subcellular location of circBLNK in OS cells was inferred by its abundance in different fractions.

Cell Counting Kit-8 (CCK-8) assay. Cell proliferation was assessed by the CCK-8 assay. In short, following the transfection of MG63 and U2OS cells with corresponding constructs

Table I. The sequences of primers used for reverse transcription-quantitative PCR.

Gene name	Primer sequence (5'→3')
CircBLNK	F: CAATGGTGGGGAATCAGTGT
	R: CTTCCATCTTCCCTCACAGC
microRNA-188-3p	F: CTCCCACATGCAGGGT
	R: GTCCAGTTTTTTTTTTTTTTTG CAA
U6	F: CTCGCTTCGGCAGCACA
	R: AACGCTTCACGAATTTGCGT
GPX4	F: TCAGCAAGATCTGCGTGAAC
	R: TCAGCAAGATCTGCGTGAAC
GAPDH	F: GTCAGTGGTGGACCTGACCT
	R: TGCTGTAGCCAAATTCGTTG

F, forward; R, reverse; GPX4, glutathione peroxidase 4.

for 72 h, the cells were collected and seeded into a 96-well plate ($1x10^4$ cells/well). After 0, 24, 48 and 72 h of cell culture, CCK-8 reagent (Thermo Fisher Scientific, Inc.) (10 μl/well) was applied and incubated for 2 h at 37˚C. The 450 nm absorbance was read by a microplate reader (Bio-Rad Laboratories, Inc.).

MTT assay. The MTT assay was used to measure cell growth capability in a 96-well plate. In short, $1x10^5$ MG63 and U2OS cells were seeded in each well. To assess the cell viability, the cells were incubated for 24 h at 37˚C. Subsequently, MTT solution (20 μl/well, 5 mg/ml) (Thermo Fisher Scientific, Inc.) was applied and incubated at 37˚C for 4 h. Subsequently, dimethyl sulfoxide (DMSO) (150 μl/well) (Invitrogen; Thermo Fisher Scientific, Inc.) was added in order to dissolve the purple formazan. Finally, the absorbance at 570 nm was calculated by an ELISA browser (BioTek EL 800; Omega Bio-Tek, Inc.).

Clonogenic assay. The cells transfected with corresponding constructs for 6 h were seeded into a six-well plate ($1x10^4$ cells/well). Then, MG63 and U2OS cells were cultured in complete DMEM supplemented with 10% FBS at 37˚C and 5% CO_2. The culture medium was replaced at 2-day intervals. After 14 days of incubation, the colonies were washed twice with phosphate-buffered saline (PBS) and fixed with 4% paraformaldehyde for 20 min. Next, 4% triformol (Invitrogen; Thermo Fisher Scientific, Inc.) was applied to fix the cells followed by the staining with 0.1% crystal violet (Beijing Solarbio Science & Technology Co.) for 20 min. Finally, the colony number with >50 cells was counted under a stereomicroscope (Olympus Corporation).

Flow cytometric analysis. Cell apoptosis of MG63 and U2OS cells was assessed by the annexin V-FITC/PI Apoptosis Detection Reagent (cat. no. 88-8102-72; Invitrogen; Thermo Fisher Scientific, Inc.) according to the manufacturer's protocol. A Beckman Coulter FACSCalibur (BD Biosciences) flow cytometer coupled with the FlowJo 7.6.1 software system (FlowJo LLC) was employed to detect apoptotic cells.

Bioinformatics analysis. The circRNA expression data was downloaded from Gene Expression Omnibus (GEO; accession no. GSE140256; URL: https://www.ncbi.nlm.nih.gov/geo/query/acc.cgi?acc=GSE140256). The binding sites between circBLNK and miR-183-3p, and the target genes of miR-183-3p were predicted using CircInteractome (URL: https://circinteractome.irp.nia.nih.gov/circular_rna.html), MicroRNA Target Prediction Database (miRDB; https://mirdb.org/) and TargetScan 7.1 database (www.targetscan.org).

Luciferase reporter assay. CircBLNK wild-type (circBLNK-WT), circBLNK mutant (circBLNK-Mut), *GPX4* wild-type (*GPX4*-WT), and *GPX4* mutant (*GPX4*-Mut) were subcloned into the pGL3-basic vector (Shanghai GeneChem Co., Ltd.). Subsequently, these constructs were co-transfected into respective 293T cell lines with mimics of miR-183-3p or control using Lipofectamine 2000 (Invitrogen; Thermo Fisher Scientific, Inc.). After 72 h, the transfected cells were harvested, and the luciferase activity of the cells was calculated by the Luciferase Reporter Assay System (Invitrogen; Thermo Fisher Scientific, Inc.). Luciferase activity was first normalized to that of *Renilla* luciferase from the same sample.

RNA pull-down assay. The RNA pull-down assay was used to validate the relationship between circBLNK and miR-188-3p. Briefly, the MG63 and U2OS cells were transfected with circBLNK probe or NC probe for 48 h at 4˚C. A total of ~$1x10^7$ cells were dissolved in the soft lysis buffer plus 80 U/ml RNasin (Promega Corporation). The probes were incubated at 4˚C for 2 h with 50 μl C-1 magnetic beads (Thermo Fisher Scientific, Inc.) to generate probe-coated beads and then incubated at 4˚C for 4 h with 0.7 ml RIPA lysis buffer (Thermo Fisher Scientific, Inc.) to lyse MG63 and U2OS cells. After washing in the lysis buffer (150 mM KCl, 25 mM Tris pH 7.4, 5 mM EDTA and 0.5% NP40), RNA complexes were subjected to centrifugation at 11,100 x g for 10 min and then eluted by denaturation in 1X protein loading buffer for 10 min at 100˚C. Finally, miR-142-3p or miR-142-5p transcripts were measured by RT-qPCR.

RNA immunoprecipitation (RIP) assay. The RIP assay was used to assess the binding of miR-188-3p to GPX4. After lysis in RIP the MG63 and U2OS cells extract was incubated with magnetic beads conjugated with anti-Ago2 (1:2,000; cat. no. ab186733; Abcam) or normal anti-IgG (1:2,000; cat. no. ab186733; Abcam) at 4˚C for 24 h. Next, the magnetic beads were treated with proteinase K, and the enrichment of miR-188-3p or GPX4 in immunoprecipitated RNAs was determined with RT-qPCR.

Ferroptosis analysis. Ferroptosis analysis was used to measure the ferroptosis cell death. In short, a mixture of 5 μM erastin (Sigma-Aldrich; Merck KGaA), 1 μM ferrostatin-1 (cat. no. 347174-05-4; Sigma-Aldrich; Merck KGaA), 25 μM Z-VAD-FMK (cat. no. V116; Sigma-Aldrich; Merck KGaA), and 20 μM necrosulfonamide (cat. no. ab143839; Abcam) was used to treat MG63 and U2OS cells at 37˚C for 24 h. Afterwards, 0.1% DMSO (Invitrogen; Thermo Fisher Scientific, Inc.) was applied to the cells followed by a 4 h incubation at 37˚C under

serum-free conditions. Finally, the cell viability was examined by the MTT assay.

Quantification of iron, malondialdehyde (MDA) and lipid reactive oxygen species (ROS). Levels of total iron and Fe^{2+} in MG63 and U2OS cells were assessed by Iron Assay kit (cat. no. ab83366; Abcam). Levels of MDA and lipid ROS were determined using Lipid Peroxidation Assay Kit (cat. no. ab118970; Abcam) and Cellular ROS Assay Kit (cat. no. ab186027; Abcam), respectively. The aforementioned kits were used according to each manufacturer's protocol.

Mitochondrial superoxide assay. MitoSOX™ Red (Thermo Fisher Scientific, Inc.) was applied to measure the production of mitochondrial superoxide in MG63 and U2OS cells. First, the working solution was prepared by diluting 5 mM MitoSOX reagent stock solution (cat. no. M36005; Thermo Fisher Scientific, Inc.) with Hanks' balanced salt solution (HBSS; Invitrogen; Thermo Fisher Scientific, Inc.). Subsequently, the working solution was applied to cells and incubated in darkness at 37˚C for 10 min. The fluorescence intensity at FL2 was measured by FACSCalibur (BD Biosciences).

Mitochondrial membrane potential assay. A Mitochondrial Membrane Potential Kit (cat. no. ab113850; Abcam) was used to measure the mitochondrial membrane potential in MG63 and U2OS cells according to the manufacturer's protocol.

Tumor formation experiment in nude mice. Subcutaneous injection was performed by Vital River Laboratories. MG63 cells ($5x10^6$) in 100 μl PBS were injected into the breast fat pads of four-week-old (weight, 15-20 g) female BALB/c nude mice (n=12). The mice were raised under a 12/12-h light/dark cycle at 18-22˚C and 50-60% humidity. Drinking water was continuously provided and food was supplemented three times a week. Both the research team and the veterinary staff monitored animal health and behavior twice daily. Tumor size was measured every three days from one week up to five weeks post-injection. Tumor volume was calculated based on the formula $V=0.5^2 \times ab^2$, where a represents tumor length and b indicates tumor width. The humane endpoint about this experiment was set to that the maximum size the tumors allowed to grow in the mice before euthanasia was 2,000 mm^3. At the end of animal experiment, the maximum tumor weight/mice weight observed was 7.4%. The maximum tumor diameter observed in this study was 16.7 mm. The duration of the experiment was five weeks. In strict accordance with the principles of animal welfare, anesthesia was used to relieve pain during euthanasia under the euthanasia by mask inhalation of isoflurane vaporized and sacrificed by cervical dislocation. Isoflurane was used at 2% for induction of anesthesia and at 1.5% for maintenance. The mice were deemed dead when the following conditions occurred: Inability to move, no spontaneous breathing, and no heartbeat. Each tumor weight was documented. The animal protocol (approval no. EC-A-2022-5-23) was approved by the Research Ethics Committee of the 970th hospital of the PLA Joint Logistic Support Force (Yantai, China).

Statistical analysis. The data were analyzed and plotted as the mean ± SD using the Prism 7.0 software (Dotmatics). Significance of differences between two groups were compared with Student's t-test, paired t-test was used in the statistical analysis of clinical samples, and the other experiments adopted unpaired t-test to analyze the difference. For multi-group data comparisons, one-way ANOVA with Tukey's post hoc test was performed. The correlations between the expression of circBLNK, miR-188-3p, and *GPX4* in OS tissues were analyzed using the Pearson's χ^2 test. The survival curves were established by the Kaplan-Meier plot (URL: https://kmplot.com/analysis/). $P<0.05$ was considered to indicate a statistically significant difference.

Results

CircBLNK is upregulated in OS tissues. The circRNA expression data was downloaded from GEO (accession no. GSE140256) (31) and the differentially expressed circRNAs in OS were detected. CircBLNK expression was observed significantly elevated in OS tissues (n=3) relative to adjacent non-cancerous specimens (n=3) (Fig. 1A and B). Furthermore, circBLNK expression in the 40 pairs of OS and adjacent non-cancerous tissues was assessed by RT-qPCR. Consistently, circBLNK level in OS tissues was significantly higher than in control tissues (Fig. 1C). Furthermore, a positive association between circBLNK expression and tumor size (Fig. 1D) and cell differentiation (Fig. 1E) was detected. Based on the median expression value of circBLNK, the 40 patients were divided into circBLNK low and high expression groups. The Kaplan-Meier analysis exhibited that high circBLNK expression was associated with poor prognosis in OS patients (Fig. 1F). Collectively, the results of the present study revealed the anomalously high expression levels of circBLNK in OS tissues, which are associated with poor OS prognosis.

Upregulation of circBLNK in OS cells promotes OS tumorigenesis. CircBLNK expression was further detected in four OS cell lines (HOS, SJSA-1, MG63 and U2OS) and a human normal osteoblast cell line (hFOB1.19). The four OS cell lines exhibited significantly higher circBLNK levels than hFOB1.19, with MG63 and U2OS cells exhibiting the highest (Fig. 2A). Afterwards, the subcellular localization of circBLNK in MG63 and U2OS cells was detected using the cell cytosolic/nuclear fractionation assay. The results revealed a specific cytoplasmic localization of circBLNK (Fig. 2B). Subsequently, the RNase R assay was used to evaluate the circular nature of circBLNK and it was revealed that RNase R efficiently digested liner BLNK but could not digest circBLNK (Fig. 2C). To dissect the role of circBLNK in OS progression, circBLNK expression in MG63 and U2OS cells was silenced by transfecting the cells with si-NC or si-circBLNK (Fig. 2D). Next, the CCK-8 and clonogenic assays were used to assess how circBLNK knockdown affected the cell proliferation ability and it was detected that the cell viability and colony-formation ability were suppressed (Fig. 2E and F). On the other hand, the cell apoptosis was enhanced when circBLNK expression was silenced (Fig. 2G). Collectively, the results of the present study revealed that circBLNK knockdown suppresses cell proliferation and enhances cell apoptosis.

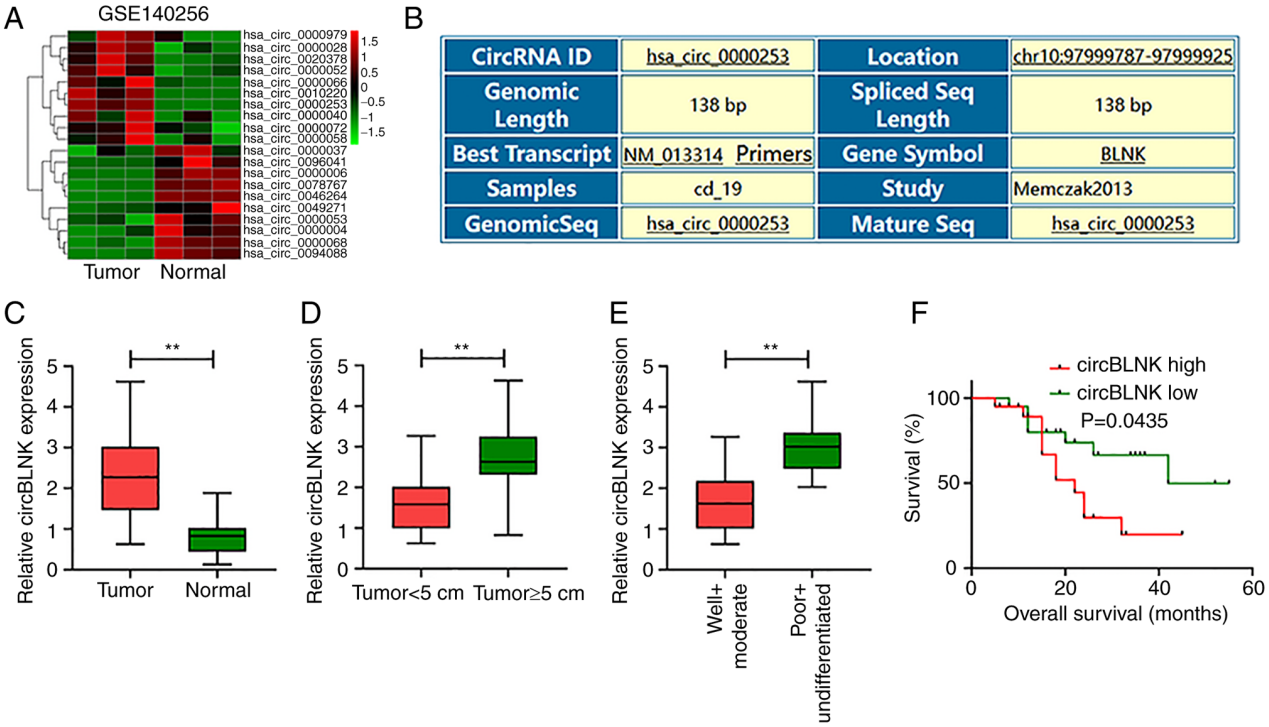

Figure 1. CircBLNK expression is elevated in OS tissues. (A) Clustered heatmap presenting differentially expressed circRNAs in three pairs of adjacent non-cancerous and OS tissues in Gene Expression Omnibus database. (B) Genomic information of circBLNK in the CircInteractome database. (C) CircBLNK expression levels in 40 pairs of adjacent non-cancerous tissues and OS tissues calculated by RT-qPCR. (D) CircBLNK expression levels at different OS tumor stages calculated by RT-qPCR. (E) CircBLNK expression levels in differentiated OS tissues calculated by RT-qPCR. (F) Kaplan-Meier survival analysis of OS patients with low or high circBLNK expression levels. All experiments were carried out in triplicate. **P<0.01. Circ-, circular; OS, osteosarcoma; RT-qPCR, reverse transcription-quantitative PCR.

CircBLNK function as a sponge of miR-188-3p. CircInteractome revealed that circBLNK could bind to miR-188-3p (Fig. 3A). The luciferase reporter and RNA pull-down assays were then performed to check this possibility. Co-transfection of WT-circBLNK with miR-188-3p mimics into 293T cells diminished the luciferase reporter activity, whereas co-transfection of MUT-circBLNK with miR-188-3p mimics retained the normal activity compared with the co-transfection with mimic control (Fig. 3B). Furthermore, using RT-qPCR, miR-188-3p expression in MG63 and U2OS cells transfected with si-NC or si-circBLNK was determined. The results demonstrated that knockdown of circBLNK increased miR-188-3p expression (Fig. 3C). In parallel, miR-188-3p transcript abundance was determined in the 40 pairs of OS and adjacent non-cancerous tissues. The abundance of miR-188-3p in OS tissues was significantly lower than in adjacent non-cancerous specimens (Fig. 3D). In addition, circBLNK expression was detected to be negetively correlated with miR-188-3p expression in OS tissues (Fig. 3E). These analyses suggested that miR-188-3p expression is subjected to the regulation by circBLNK. Next, for the collection of direct evidence supporting that circBLNK targets miR-188-3p, the RNA pull-down assay was performed. The assay detected the enrichment of miR-188-3p in the circBLNK probe fraction compared with the NC probe fraction (Fig. 3F). Taken together, these findings indicated that circBLNK regulates the OS tumorigenesis by sponging miR-188-3p.

GPX4 is a direct target of miR-188-3p. The miRDB revealed a high possibility that miR-188-3p bind to *GPX4* (Fig. 4A). The luciferase reporter assay was then performed to validate this interaction. Co-transfection of miR-188-3p mimics and WT-*GPX4* resulted in weaker luciferase reporter activity in 293T cells, whereas the cells co-transfected with miR-188-3p mimics and MUT-*GPX4* showed normal luciferase reporter activity (Fig. 4B). Moreover, the RIP assay displayed that both miR-188-3p and *GPX4* were effectively pulled down by Ago2, indicating the direct interaction between them (Fig. 4C and D). Afterwards, *GPX4* expression was measured in the 40 pairs of OS and adjacent non-cancerous tissues by RT-qPCR. GPX4 expression was significantly elevated in OS tissues (Fig. 4E). Additionally, a positive correlation was detected between the abundance of circBLNK and *GPX4*, whereas a negative correlation was found between the abundance of miR-188-3p and *GPX4* in OS tissues (Fig. 4F). Moreover, the levels of GPX4 transcripts and protein were all diminished in MG63 and U2OS cells transfected with si-circBLNK, which was reversed with the presence of miR-188-3p inhibitor (Fig. 4G and H). Furthermore, circBLNK knockdown suppressed the proliferation but enhanced the cell apoptosis of MG63 and U2OS cells, while these effects were reversed with the presence of miR-188-3p inhibitor (Fig. 4I and J). In summary, the results of the present study demonstrated that circBLNK promotes OS progression by regulating the miR-188-3p/GPX4 pathway.

CircBLNK inhibits ferroptosis in OS cells by regulating the miR-188-3p/GPX4 signaling. Finally, the regulation of ferroptosis by the circBLNK/miR-188-3p/GPX4 signaling was investigated in OS cells. First, with the use of MTT assay,

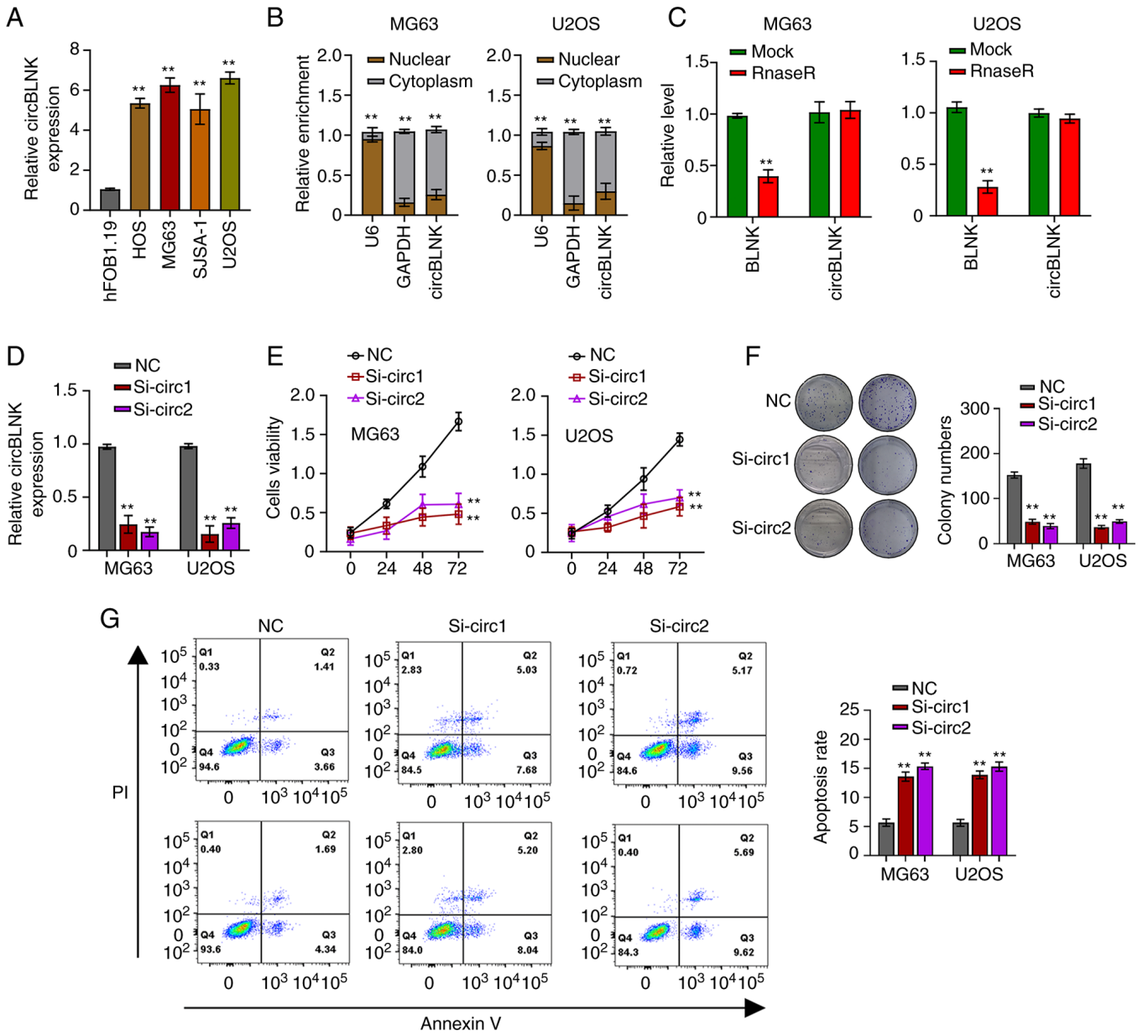

Figure 2. CircBLNK expression is elevated in OS cell lines and promotes OS tumorigenesis. (A) CircBLNK expression levels in four OS cell lines (HOS, SJSA-1, MG63 and U2OS) and a human normal osteoblast cell line (hFOB1.19) calculated using RT-qPCR. (B) Subcellular location of circBLNK in OS cell lines (MG63 and U2OS) determined using the cell cytosolic/nuclear fractionation assay. (C) Expression levels of circBLNK and BLNK in OS cell lines (MG63 and U2OS) with or without RNase R treatment calculated using RT-qPCR. (D) Expression levels of circBLNK in OS cell lines (MG63 and U2OS) transfected with si-NC or si-circBLNK (si-circ1 and si-circ2) assessed using RT-qPCR. (E) Cell proliferation was determined using Cell Counting Kit-8 assay. (F) Colony number of cells in was calculated using clonogenic assay. (G) Numbers of apoptotic cells were calculated by flow cytometry analysis. All experiments were carried out in triplicate. **P<0.01. Circ-, circular; OS, osteosarcoma; RT-qPCR, reverse transcription-quantitative PCR; si-, small interfering; NC, negative control.

erastin, a ferroptosis inducer, was verified to activate cell death in MG63 and U2OS cells, whereas ferrostain-1, a ferroptosis inhibitor, could counteract the effect of erastin (Fig. 5A). Of note, ZVAD-FMK (apoptosis inhibitor) and necrosulfonamide (necroptosis inhibitor) did not affect the induction of cell death by erastin (Fig. 5A). Afterwards, using the MTT assay, the way circBLNK/miR-188-3p/GPX4 signaling affects ferroptosis induction by erastin was investigated. The percentage of cells undergoing cell death was revealed to be increased by circBLNK knockdown, an effect that was reversed by OE-GPX4-overexpressing cells (Fig. 5B). Since cell death is dependent on intracellular iron (Fe^{2+}) level, it was then assessed whether the circBLNK/miR-188-3p/GPX4 signaling affects the intracellular Fe^{2+} level in MG63 andU2OS cells. The concentration of Fe^{2+} was demonstrated to be increased when circBLNK was knocked down, which was rescued by GPX4-overexpressing cells (Fig. 5C and D). Furthermore, circBLNK knockdown resulted in an enhancement of MDA and lipid ROS generation, which was reversed by GPX4-overexpressing cells (Fig. 5E and F). In the cells with circBLNK knockdown, the mitochondrial superoxide concentration was increased, while the mitochondrial membrane potential was diminished, which were eliminated by GPX4-overexpressing cells (Fig. 5G and H). These results

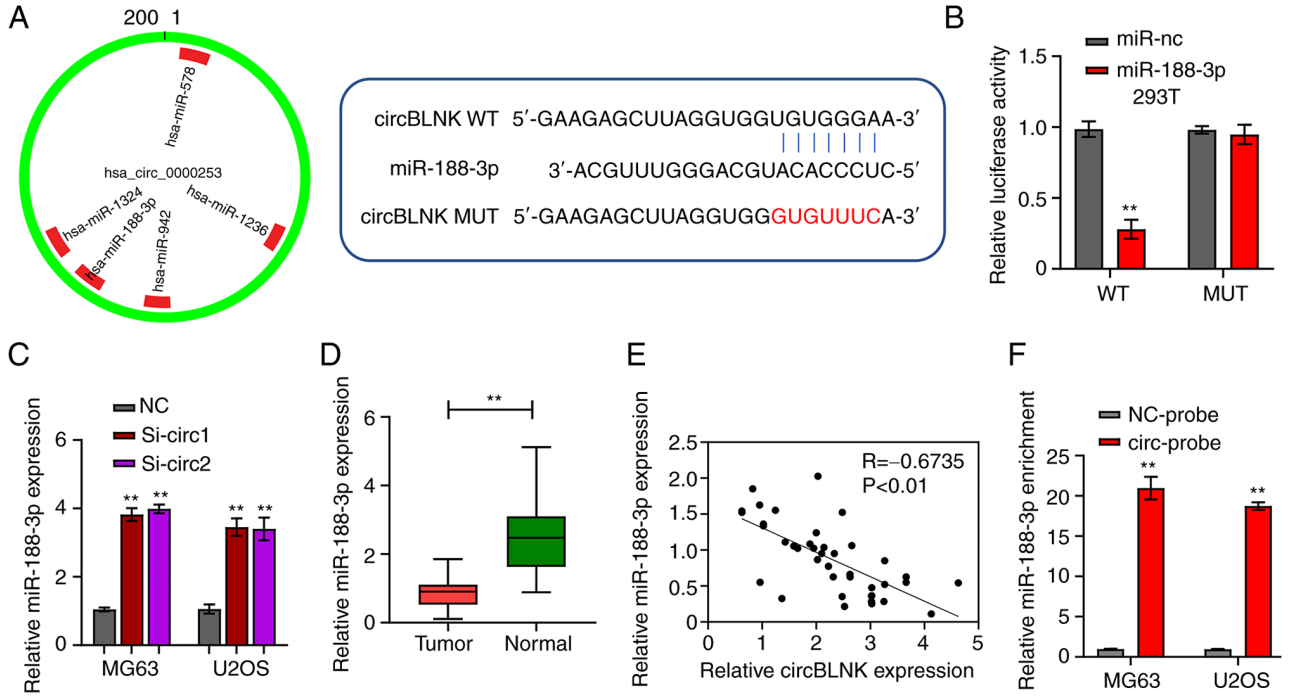

Figure 3. CircBLNK functions as a sponge of miR-188-3p. (A) Putative complementary sequences of circBLNK and miR-188-3p. (B) Relationship between circBLNK and miR-188-3p was examined by luciferase reporter assay. (C) miR-188-3p expression levels in OS cell lines (MG63 and U2OS) transfected with si-NC or si-circBLNK (si-circ1 and si-circ2) were calculated by RT-qPCR. (D) Interaction between circBLNK and miR-188-3p was determined using RNA pull-down assay. (E) miR-188-3p expression levels in 40 pairs of OS and adjacent non-cancerous tissues were assessed using RT-qPCR. (F) Correlation between the expression of circBLNK and miR-188-3p in OS tissues was analyzed using Pearson's correlation coefficient. All experiments were carried out in triplicate. **P<0.01. Circ-, circular; miR, microRNA; OS, osteosarcoma; RT-qPCR, reverse transcription-quantitative PCR; si-, small interfering; NC, negative control.

suggested that circBLNK inhibits ferroptosis by regulating the miR-188-3p/GPX4 signaling in OS cells.

CircBLNK knockdown inhibits OS tumor growth. To confirm circBLNK is a *bona fide* tumor promoter *in vivo*, MG63 cells stably transfected with si-NC or si-circBLNK were used to inject nude mice subcutaneously. Tumor volume detection revealed a significant decrease in subcutaneous tumor volume in the si-circBLNK group vs. the si-NC group (Fig. S1A). Similarly, circBLNK knockdown significantly reduced the tumor weight (Fig. S1B). Collectively, the aforementioned data suggested that circBLNK promotes OS tumor growth *in vivo*.

Discussion

With the advent of high-throughput genomic and RNA sequencing, a large array of circRNAs have been identified. Over the past decades, the pivotal role of circRNAs in malignant tumor tumorigenesis has been well documented (32,33). In the present study, the role of circBLNK in OS progression was molecularly dissected. CircBLNK was elevated in both OS tissues and cell lines, facilitating the proliferation while impairing the apoptosis and ferroptosis of OS cells. Altogether, the circBLNK/miR-188-3p/GPX4 axis was identified as a new transcriptional regulatory network for OS progression.

CircBLNK is a newly discovered circRNA, located in chromosome 10. In the present study, circBLNK expression was revealed to be elevated in OS tissues and this was associated with large tumor size, low cell differentiation and poor prognosis. Then, the use of RT-qPCR confirmed the elevated circBLNK expression in both OS tissues and cell lines. Moreover, it was observed that circBLNK knockdown impaired OS cell proliferation while enhancing cell apoptosis. These results suggested that circBLNK may play a facilitating role in OS tumorigenesis and progression.

CircRNAs exert their functions through sponging miRNAs (34,35). It was observed that circRNAs are involved in OS progression by sponging miRNAs. For instance, circCAMSAP1 promotes OS development through sponging miR-145-5p (36), hsa_circ_0008259 regulates OS progression by sponging miR-21-5p (37), circEIF4G2 accelerates OS tumorigenesis and progression by sponging miR-218 (38). In the present study, it was demonstrated that miR-188-3p is the target for circBLNK. MiR-188-3p expression was downregulated in many malignant tumor tissues (39-41). Congruent with the aforementioned findings of previous studies, it was also observed that miR-188-3p was downregulated in OS tissues. In addition, the results of the present study confirmed that circBLNK deficiency impaired OS cell proliferation, while enhancing cell apoptosis, and both phenotypes could be reversed by inhibiting miR-188-3p. Collectively, these results demonstrated that circBLNK regulates the OS tumorigenesis through sponging miR-188-3p.

CircRNAs typically act as ceRNAs to modulate the expression of target miRNA (42). In the present study, through a combination of bioinformatics prediction, luciferase reporter assay, and RIP assay, *GPX4* was demonstrated as the target gene of miR-188-3p. Furthermore, the level of *GPX4* transcripts was

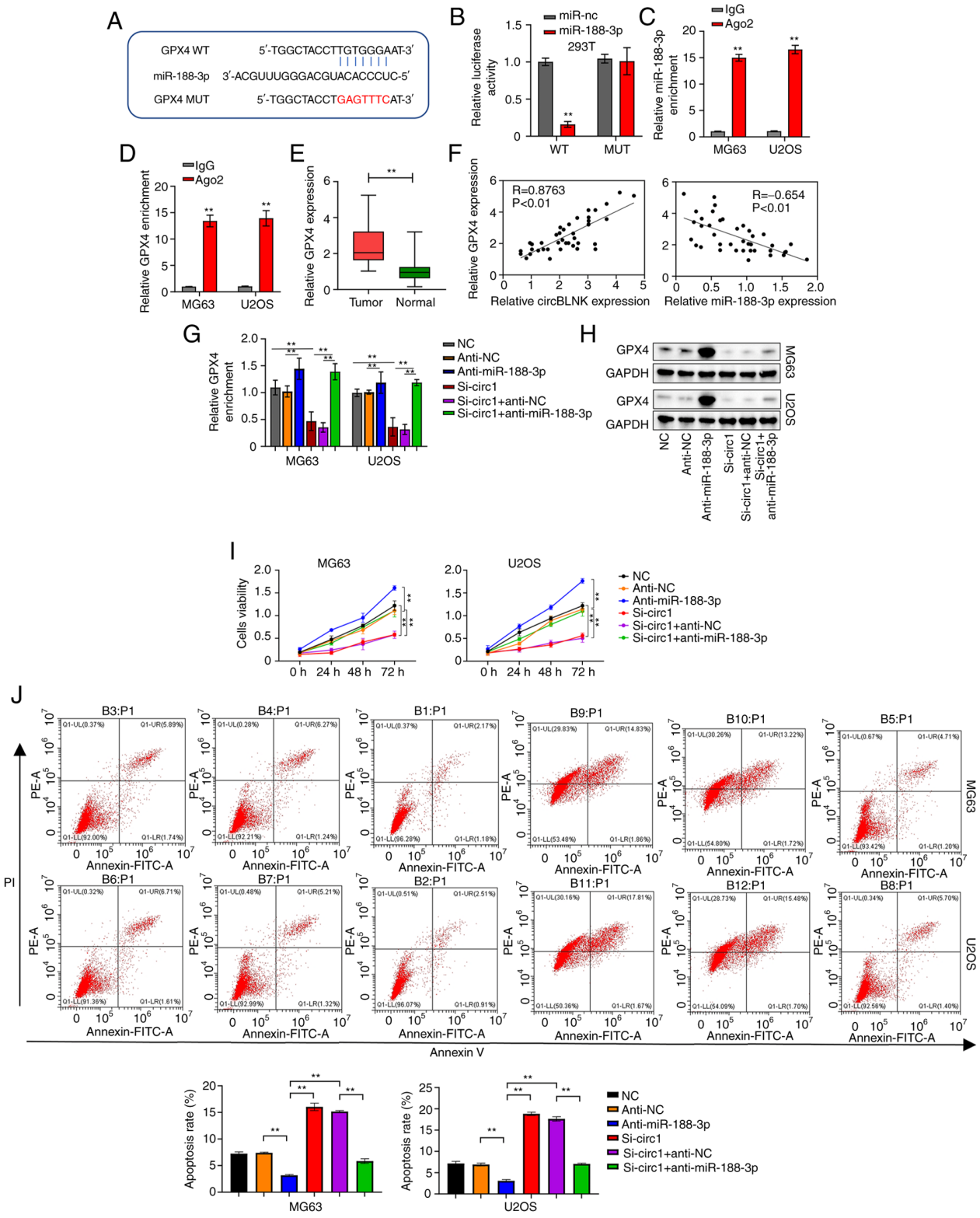

Figure 4. GPX4 is a direct target of miR-188-3p. (A) Complementary sequences of miR-188-3p and *GPX4* predicted by the miRDB database. (B) Relationship between miR-188-3p and GPX4 confirmed by luciferase reporter assay. (C) Interaction between miR-188-3p and GPX4 determined using RIP assay. (D) Relationship between miR-188-3p and GPX4 assessed using RIP assay. (E) GPX4 expression levels in 40 pairs of adjacent non-cancerous and OS tissues was calculated using RT-qPCR. (F) The correlation between the expression levels of circBLNK and GPX4 or miR-188-3p and GPX4 in OS tissues was analyzed by the Pearson's correlation coefficient. (G) GPX4 expression levels in OS cell lines (MG63 and U2OS) transfected with indicated constructs (si-NC, anti-NC, anti-miR-188-3p, si-circBLNK, si-circBLNK + anti-NC, and si-circBLNK+anti-miR-188-3p) was calculated by RT-qPCR. (H) Protein levels of GPX4 in OS cell lines (MG63 and U2OS) transfected with indicated constructs (si-NC, anti-NC, anti-miR-188-3p, si-circBLNK, si-circBLNK + inhibitor control, and si-circBLNK+miR-188-3p inhibitor) calculated by western blot. (I) Cell proliferation in OS cell lines (MG63 and U2OS) transfected with indicated constructs (si-NC, anti-NC, anti-miR-188-3p, si-circBLNK, si-circBLNK + anti-NC, and si-circBLNK + anti-miR-188-3p) was calculated by Cell Counting Kit-8 assay. (J) Number of apoptotic cells in OS cell lines (MG63 and U2OS) transfected with indicated constructs (si-NC, anti-NC, anti-miR-188-3p, si-circBLNK, si-circBLNK + anti-NC and si-circBLNK + anti-miR-188-3p) was calculated by flow cytometric analysis. All experiments were carried out in triplicate. **P<0.01. GPX4, glutathione peroxidase 4; miR, microRNA; miRDB, MicroRNA Target Prediction Database; OS, osteosarcoma; RT-qPCR, reverse transcription-quantitative PCR; RIP, RNA immunoprecipitation; si-, small interfering; NC, negative control.

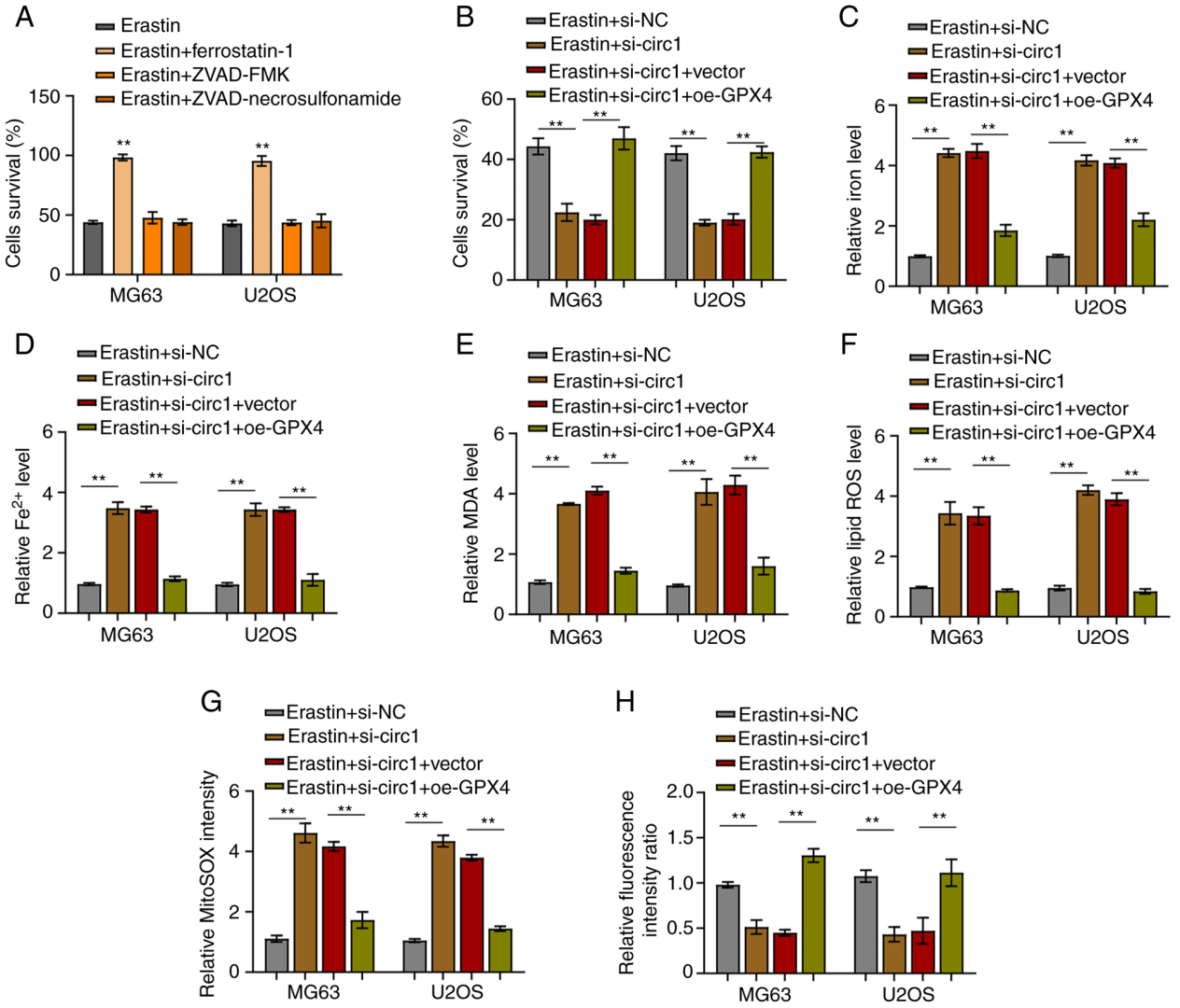

Figure 5. CircBLNK inhibits ferroptosis in OS cells through regulating the microRNA-188-3p/GPX4 signaling. (A) Cell growth in OS cell lines (MG63 and U2OS) treated with indicated constructs (Erastin, Erastin + ferrostatin-1, Erastin + ZVAD-FMK and Erastin + necrosulfonamide) was evaluated by MTT assay. (B) Cell growth in OS cell lines (MG63 and U2OS) treated with indicated constructs (Erastin + si-NC, Erastin + si-circBLNK, Erastin + si-circBLNK + OE-vector, and Erastin + si-circBLNK + OE-GPX4) was assessed by MTT assay. (C) Expression level of total iron levels in was determined through an iron assay kit. (D) Fe^{2+} accumulation was assessed by an iron assay kit. (E) MDA level was determined by lipid peroxidation assay. (F) Lipid ROS level was detected using flow cytometric analysis. (G) Mitochondrial superoxide concentration was determined by mitochondrial superoxide assay. (H) Mitochondrial membrane potential was evaluated using mitochondrial membrane potential assay. All experiments were carried out in triplicate. **P<0.01. Circ-, circular; OS, osteosarcoma; si-, small interfering; NC, negative control; OE, overexpression; MDA, malondialdehyde; ROS, reactive oxygen species; GPX4, glutathione peroxidase 4.

determined to be elevated in OS tissues. Moreover, a positive correlation of *GPX4* expression with circBLNK expression was observed, and a negative correlation between *GPX4* expression and miR-188-3p expression was also identified. Thus, it was demonstrated that circBLNK functions as a ceRNA for miR-188-3p to regulate GPX4 expression.

Ferroptosis has emerged as a new form of cell death mediated by peroxidation of ROS and lipid (43). Ferroptosis-based therapy has been proposed as an alternative treatment for malignant tumor treatment (44). Sorafenib, an FDA-approved small molecule drug for cancer therapy, is an inducer of ferroptosis (45). Other than Sorafenib, gene therapies based on ferroptosis-associated nanomaterials are undergoing development (46). It has been revealed that ferroptosis is tightly associated with the progression of diverse malignant tumors including OS (27,47,48). In the present study, it was identified that circBLNK silencing augmented ferroptosis as reflected by the elevated levels of intracellular Fe^{2+}, MDA, lipid ROS and mitochondrial superoxide as well as the diminished mitochondrial membrane potential. This enhancement of ferroptosis by circBLNK silencing could be eliminated in OE-GPX4-overexpressing cells. Collectively, these results demonstrated that circBLNK inhibits OS cell ferroptosis through the miR-188-3p/GPX4 signaling. In conclusion, the present study investigated the upregulation of circBLNK in OS tissues and cells, which predicts poor patient prognosis. Mechanistically, circBLNK functions as a ceRNA to arrest miR-188-3p expression and to upregulate GPX4 expression, thereby ultimately promoting OS tumorigenesis. Meanwhile, the present study provided a potential molecular target for OS early diagnosis and therapeutic interventions.

Acknowledgements

Not applicable.

Funding

The present study was supported by PLA Youth Training Project for Medical Science (grant no. 17QNP015).

Availability of data and materials

The datasets used and/or analyzed during the current study are available from the corresponding author on reasonable request.

Authors' contributions

DXH and WPS made substantial contributions to conception and design. ZJL, YL and CBW performed the experiments and acquired the data. ZJL and CBW analyzed the data. DXH and YL drafted the manuscript. ZJL and CBW critically revised the study for important intellectual content. DXH and WPS confirm the authenticity of all the raw data. All authors read and approved the final version of the manuscript and agreed to be accountable for all aspects of the work.

Ethics approval and consent to participate

Human studies (approval no. EC-H-2021-12-16) and animal experiments (approval no. EC-A-2022-5-23) were approved by the Research Ethics Committee of the 970th hospital of the PLA Joint Logistic Support Force (Yantai, China). All patients were informed of the research design and written informed consent was provided by all patients.

Patient consent for publication

Not applicable.

Competing interests

The authors declare that they have no competing interests.

References

1. Noone AM, Cronin KA, Altekruse SF, Howlader N, Lewis DR, Petkov VI and Penberthy L: Cancer incidence and survival trends by subtype using data from the surveillance epidemiology and end results program, 1992-2013. Cancer Epidemiol Biomarkers Prev 26: 632-641, 2017.
2. Rainusso N, Wang LL and Yustein JT: The adolescent and young adult with cancer: State of the Art-bone tumors. Curr Oncol Rep 15: 296-307, 2013.
3. Ottaviani G and Jaffe N: The epidemiology of osteosarcoma. Cancer Treat Res 152: 3-13, 2009.
4. Bishop MW, Janeway KA and Gorlick R: Future directions in the treatment of osteosarcoma. Curr Opin Pediatr 28: 26-33, 2016.
5. Otoukesh B, Boddouhi B, Moghtadaei M, Kaghazian P and Kaghazian M: Novel molecular insights and new therapeutic strategies in osteosarcoma. Cancer Cell Int 18: 158, 2018.
6. Bielack SS, Kempf-Bielack B, Delling G, Exner GU, Flege S, Helmke K, Kotz R, Salzer-Kuntschik M, Werner M, Winkelmann W, *et al*: Prognostic factors in high-grade osteosarcoma of the extremities or trunk: An analysis of 1,702 patients treated on neoadjuvant cooperative osteosarcoma study group protocols. J Clin Oncol 20: 776-790, 2002.
7. Kristensen LS, Andersen MS, Stagsted LVW, Ebbesen KK, Hansen TB and Kjems J: The biogenesis, biology and characterization of circular RNAs. Nat Rev Genet 20: 675-691, 2019.
8. Li J, Sun D, Pu W, Wang J and Peng Y: Circular RNAs in cancer: Biogenesis, function, and clinical significance. Trends Cancer 6: 319-336, 2020.
9. Liu Z, Liu F, Wang F, Yang X and Guo W: CircZNF609 promotes cell proliferation, migration, invasion, and glycolysis in nasopharyngeal carcinoma through regulating HRAS via miR-338-3p. Mol Cell Biochem 476: 175-186, 2021.
10. Fan C, Qu H, Xiong F, Tang Y, Tang T, Zhang L, Mo Y, Li X, Guo C, Zhang S, *et al*: CircARHGAP12 promotes nasopharyngeal carcinoma migration and invasion via ezrin-mediated cytoskeletal remodeling. Cancer Lett 496: 41-56, 2021.
11. Wang L, Tong X, Zhou Z, Wang S, Lei Z, Zhang T, Liu Z, Zeng Y, Li C, Zhao J, *et al*: Circular RNA hsa_circ_0008305 (circPTK2) inhibits TGF-β-induced epithelial-mesenchymal transition and metastasis by controlling TIF1γ in non-small cell lung cancer. Mol Cancer 17: 140, 2018.
12. Li C, Tian Y, Liang Y and Li Q: Retraction note to: Circ_0008035 contributes to cell proliferation and inhibits apoptosis and ferroptosis in gastric cancer via miR-599/EIF4A1 axis. Cancer Cell Int 21: 416, 2021.
13. Li ZQ, Wang Z, Zhang Y, Lu C, Ding QL, Ren R, Cheng BB and Lou LX: CircRNA_103801 accelerates proliferation of osteosarcoma cells by sponging miR-338-3p and regulating HIF-1/Rap1/PI3K-Akt pathway. J Biol Regul Homeost Agents 35: 1021-1028, 2021.
14. Gong G, Han Z, Wang W, Xu Q and Zhang J: Silencing hsa_circRNA_0008035 exerted repressive function on osteosarcoma cell growth and migration by upregulating microRNA-375. Cell Cycle 19: 2139-2147, 2020.
15. Liu DY, Li Z, Zhang K, Jiao N, Lu DG, Zhou DW, Meng YB and Sun L: Circular RNA CircMTO1 suppressed proliferation and metastasis of osteosarcoma through miR-630/KLF6 axis. Eur Rev Med Pharmacol Sci 25: 86-93, 2021.
16. Thomson DW and Dinger ME: Endogenous microRNA sponges: Evidence and controversy. Nat Rev Genet 17: 272-283, 2016.
17. Zheng S, Jiang F, Ge D, Tang J, Chen H, Yang J, Yao Y, Yan J, Qiu J, Yin Z, *et al*: LncRNA SNHG3/miRNA-151a-3p/RAB22A axis regulates invasion and migration of osteosarcoma. Biomed Pharmacother 112: 108695, 2019.
18. Zhang W, Li JZ, Tai QY, Tang JJ, Huang YH and Gao SB: LncRNA DANCR regulates osteosarcoma migration and invasion by targeting miR-149/MSI2 axis. Eur Rev Med Pharmacol Sci 24: 6551-6560, 2020.
19. Xu M, Zhang YY, Wang HF and Yang GS: The expression and function of miRNA-106 in pediatric osteosarcoma. Eur Rev Med Pharmacol Sci 21: 715-722, 2017.
20. Luo Z, Fan Y, Liu X, Liu S, Kong X, Ding Z, Li Y and Wei L: MiR-188-3p and miR-133b suppress cell proliferation in human hepatocellular carcinoma via post-transcriptional suppression of NDRG1. Technol Cancer Res Treat 20: 15330338211033074, 2021.
21. Pei J, Zhang S, Yang X, Han C, Pan Y, Li J, Wang Z, Sun C and Zhang J: Long non-coding RNA RP11-283G6.5 confines breast cancer development through modulating miR-188-3p/TMED3/Wnt/β-catenin signalling. RNA Biol 18 (Suppl 1): S287-S302, 2021.
22. Pei J, Zhang J, Yang X, Wu Z, Sun C, Wang Z and Wang B: TMED3 promotes cell proliferation and motility in breast cancer and is negatively modulated by miR-188-3p. Cancer Cell Int 19: 75, 2019.
23. Seiler A, Schneider M, Förster H, Roth S, Wirth EK, Culmsee C, Plesnila N, Kremmer E, Rådmark O, Wurst W, *et al*: Glutathione peroxidase 4 senses and translates oxidative stress into 12/15-lipoxygenase dependent- and AIF-mediated cell death. Cell Metab 8: 237-248, 2008.
24. Yang WS, SriRamaratnam R, Welsch ME, Shimada K, Skouta R, Viswanathan VS, Cheah JH, Clemons PA, Shamji AF, Clish CB, *et al*: Regulation of ferroptotic cancer cell death by GPX4. Cell 156: 317-331, 2014.
25. Stockwell BR, Friedmann Angeli JP, Bayir H, Bush AI, Conrad M, Dixon SJ, Fulda S, Gascón S, Hatzios SK, Kagan VE, *et al*: Ferroptosis: A regulated cell death nexus linking metabolism, redox biology, and disease. Cell 171: 273-285, 2017.
26. Xu Z, Chen L, Wang C, Zhang L and Xu W: MicroRNA-1287-5p promotes ferroptosis of osteosarcoma cells through inhibiting GPX4. Free Radic Res 55: 1119-1129, 2021.

27. Liu Q and Wang K: The induction of ferroptosis by impairing STAT3/Nrf2/GPx4 signaling enhances the sensitivity of osteosarcoma cells to cisplatin. Cell Biol Int 43: 1245-1256, 2019.
28. Issue Information-declaration of Helsinki. J Bone Miner Res 34: BM i-BM ii, 2019.
29. Livak KJ and Schmittgen TD: Analysis of relative gene expression data using real-time quantitative PCR and the 2(-Delta Delta C(T)) method. Methods 25: 402-408, 2001.
30. Zheng X, Huang M, Xing L, Yang R, Wang X, Jiang R, Zhang L and Chen J: The circRNA circSEPT9 mediated by E2F1 and EIF4A3 facilitates the carcinogenesis and development of triple-negative breast cancer. Mol Cancer 19: 73, 2020.
31. Xu L, Duan J, Li M, Zhou C and Wang Q: Circ_0000253 promotes the progression of osteosarcoma via the miR-1236-3p/SP1 axis. J Pharm Pharmacol 75: 227-235, 2023.
32. Meng S, Zhou H, Feng Z, Xu Z, Tang Y, Li P and Wu M: CircRNA: Functions and properties of a novel potential biomarker for cancer. Mol Cancer 16: 94, 2017.
33. Wang D, Yang S, Wang H, Wang J, Zhang Q, Zhou S, He Y, Zhang H, Deng F, Xu H, *et al*: The progress of circular RNAs in various tumors. Am J Transl Res 10: 1571-1582, 2018.
34. Yang Y, Yujiao W, Fang W, Linhui Y, Ziqi G, Zhichen W, Zirui W and Shengwang W: The roles of miRNA, lncRNA and circRNA in the development of osteoporosis. Biological Res 53: 40, 2020.
35. Patop IL, Wüst S and Kadener S: Past, present, and future of circRNAs. EMBO J 38: e100836, 2019.
36. Chen Z, Xu W, Zhang D, Chu J, Shen S, Ma Y, Wang Q, Liu G, Yao T, Huang Y, *et al*: circCAMSAP1 promotes osteosarcoma progression and metastasis by sponging miR-145-5p and regulating FLI1 expression. Mol Ther Nucleic Acids 23: 1120-1135, 2021.
37. Guan K, Liu S, Duan K, Zhang X, Liu H, Xu B, Wang X and Jin X: Hsa_circ_0008259 modulates miR-21-5p and PDCD4 expression to restrain osteosarcoma progression. Aging (Albany NY) 13: 25484-25495, 2021.
38. Lin E, Liu S, Xiang W, Zhang H and Xie C: CircEIF4G2 Promotes Tumorigenesis and Progression of Osteosarcoma by Sponging miR-218. Biomed Res Int 2020: 8386936, 2020.
39. Meng L, Jiang YP, Zhu J and Li B: MiR-188-3p/GPR26 modulation functions as a potential regulator in manipulating glioma cell properties. Neurol Res 42: 222-227, 2020.
40. Pichler M, Stiegelbauer V, Vychytilova-Faltejskova P, Ivan C, Ling H, Winter E, Zhang X, Goblirsch M, Wulf-Goldenberg A, Ohtsuka M, *et al*: Genome-Wide miRNA analysis identifies miR-188-3p as a novel prognostic marker and molecular factor involved in colorectal carcinogenesis. Clin Cancer Res 23: 1323-1333, 2017.
41. Gao F, Han J, Wang Y, Jia L, Luo W and Zeng Y: Circ_0109291 promotes cisplatin resistance of oral squamous cell carcinoma by sponging miR-188-3p to increase ABCB1 expression. Cancer Biother Radiopharm 37: 233-245, 2022.
42. Saliminejad K, Khorram Khorshid HR, Soleymani Fard S and Ghaffari SH: An overview of microRNAs: Biology, functions, therapeutics, and analysis methods. J Cell Physiol 234: 5451-5465, 2019.
43. Hassannia B, Vandenabeele P and Vanden Berghe T: Targeting ferroptosis to iron out cancer. Cancer Cell 35: 830-849, 2019.
44. Chen X, Kang R, Kroemer G and Tang D: Broadening horizons: The role of ferroptosis in cancer. Nat Rev Clin Oncol 18: 280-296, 2021.
45. Liang C, Zhang X, Yang M and Dong X: Recent progress in ferroptosis inducers for cancer therapy. Adv Mater 31: e1904197, 2019.
46. Sun X, Ou Z, Chen R, Niu X, Chen D, Kang R and Tang D: Activation of the p62-Keap1-NRF2 pathway protects against ferroptosis in hepatocellular carcinoma cells. Hepatology 63: 173-184, 2016.
47. Lei T, Qian H, Lei P and Hu Y: Ferroptosis-related gene signature associates with immunity and predicts prognosis accurately in patients with osteosarcoma. Cancer Sci 112: 4785-4798, 2021.
48. Luo Y, Gao X, Zou L, Lei M, Feng J and Hu Z: Bavachin induces ferroptosis through the STAT3/P53/SLC7A11 axis in osteosarcoma cells. Oxid Med Cell Longev 2021: 1783485, 2021.